MICROPLASMA ANTENNAS: CHARACTERIZING CAPILLARY PLASMA DISCHARGES AS POTENTIAL MONOPOLE ANTENNAS

BY

KYLE THOMAS RAYMOND

THESIS

Submitted in partial fulfillment of the requirements
for the degree of Master of Science in Electrical and Computer Engineering
in the Graduate College of the
University of Illinois at Urbana-Champaign, 2016

Urbana, Illinois

Adviser:

Professor J. Gary Eden

ABSTRACT

This thesis investigates the use of capillary plasma elements, in glass and quartz with sub-millimeter inner diameters and 1–5 cm in length, as monopole antenna elements. Plasma elements of this size have not been demonstrated before, as most plasma antennas use fluorescent tubes with inner diameters greater than 2 cm and longer than 30 cm. In order to validate that capillary plasma elements function well as the conductive element in antenna structures, spectroscopic electron density measurements of the Stark broadening in the Balmer series were performed for two capillary antenna elements. Glass tubes operated as a dielectric barrier discharge, or DBD, driven by an AC voltage of 10–40 kHz showed peak electron densities of $n_e = 10^{15}$ cm^{-3}. Time-averaged electron densities and conductivities in these tubes remained well below $n_e = 10^{14}$ cm^{-3} and $\sigma_p = 100$ S/m, two threshold values for adequate antenna operation. Quartz tubes driven by a 140 MHz RF voltage maintained time-averaged electron densities of $8{\times}10^{14}$ cm^{-3}. This result indicates that capillary microplasma discharges in capillary tubes can be used as monopole antennas with electronically variable resonances and radiation patterns, as well as the opportunity to investigate microplasma monopole elements incorporated into arrays once the engineering problems of plasma breakdown and stability have been solved.

To my parents, for their love and support.
To my wife, for her wisdom.
To giants, for their shoulders.

ACKNOWLEDGMENTS

This thesis would not exist without the guidance and support of the people who are LOPE, the Laboratory of Optical Physics and Engineering.

Thank you, Dr. Gary Eden, for your exuberant pursuit of scientific truth, for your kindness and encouragement in coursework and in the lab, and for your wellspring of ideas. I would not be a scientist and engineer today without conversations we had before I started at Parkland, during my second undergrad degree, and during these past two years. It has been a blessing to work with and for you.

Thank you, Dr. Tom Houlahan, for your love of scientific rigor, your courage in the face of new experiments, your enthusiasm, and your friendship in and out of the lab. Working with you and discussing these experiments helped me grow as a scientist. Hanging out with you helped me grow as a person.

Thank you, LOPE! You have all taught me how to think, persevere, laugh, throw gators, counterstrike, and ignite copper tape into perfect flames.

Of course, I would not have considered returning to school if not for my parent's generosity, both financially and emotionally. Mother and Father, thank you for being steady rocks of unconditional love. I'll see you soon.

And thank you, Jen, for a new and better world, a world which includes lasers, plasmas, and many nights of paper-writing — you made it delightful. Love you.

TABLE OF CONTENTS

LIST OF SYMBOLS

n_e	Electron Density
υ_m	Electron-neutral Collisional Frequency
ω_{pe}	Electron Plasma Frequency
ω_{pi}	Ion Plasma Frequency
f_d	Plasma Driving Frequency

CHAPTER 1

INTRODUCTION

Antenna theory is a relatively mature field of study, established in the theoretical work of James Clerk Maxwell in the 1860s and demonstrated experimentally by Heinrich Hertz in 1887 [1]. In the 20th century antenna theory matured, adding arrays, horns, reflectors, apertures, microstrips, satellites, and cell networks to the wireless communications [2]. Antenna theorists experimented with the geometry of antennas, the number of antenna structures, and the phase of antenna excitation to produce flexible communication systems capable of covering a broad design space.

Until the 1960s antennas were strictly made with metal. Metal structures provided ample free electrons, which in turn allowed currents to flow on the antenna structure. However, in the 1960s, experiments by Askar'yan and Raevskii confirmed that plasmas could be used in place of metal in antenna structures [1]. Plasmas as alternative antenna structures were studied by the Naval Research Laboratory in the United States in the 1990s, developing reflector plasma antennas. Transmission and reception, reconfigurability, and stealth properties have all been demonstrated experimentally [3].

Plasma antennas provide a few advantages over metal antennas. Typically, a plasma antenna is a discharge bounded by a dielectric. If the plasma is not energized, the antenna structure disappears and is invisible to other wireless systems. Electronic control of the plasma discharge allows for control of antenna parameters like resonance frequency and transparency. Plasma antennas can be reconfigured and switched in less than 1 μs [4]. Plasma antennas have been demonstrated to operate at 30 MHz to 20 GHz, in tubes and surface plasmas, and at 5 W of discharge power [3].

Despite these promising results, plasma antennas have remained strictly research devices. First, plasma antennas require power to operate, a distinct disadvantage against metal antennas, and in some cases require magnetic fields larger than 100 G to maintain. Further, operating frequencies in plasma

antennas are limited by the electron density [4]. Due to the correspondence of frequency and physical size in antennas, plasma antennas tend to be large, bulky pieces of fragile equipment with glass tubes on the order of a meter in length and >3 cm in diameter.

Microplasma discharges offer an antenna engineer smaller devices only centimeters in length and less than a millimeter in diameter operating at higher pressures (and therefore higher potential electron densities) while maintaining low overall device temperatures. If a single capillary tube plasma discharge operating with higher electron densities in smaller structures can operate as an antenna, plasma antennas will be able to expand into new frequency regimes, new power regimes, and, hopefully, new and practical applications.

This thesis introduces the basic plasma theory necessary for antenna operation and the development and characterization of two potential capillary plasma systems. The first potential device is a capacitively coupled capillary tube of glass (1 mm ID, 4 cm long) filled with a noble gas driven with a 20 kHz, 3 kVp-p sinusoidal waveform. Spectroscopic measurement of instantaneous electron densities above 10^{14} cm^{-3} in these devices gave conductivities above 50 S/m. However, when reflection parameters, or the S11, were measured with the device installed in a calibrated antenna structure, no shift in resonance was observed when the plasma was cycled on and off. This result suggested that while the instantaneous electron density was over 10^{14} cm^{-3}, the average electron density was lower.

The second proposed device was designed to increase the time-averaged electron density. It is hoped that by creating a discharge in alumina or quartz tubes (.5 mm ID, 4 cm long) driven at higher frequencies (100 MHz), the time-averaged electron density will increase to above 10^{14} cm^{-3}. Alumina or sapphire tubes are much more robust, able to withstand higher power deposition than glass tubes. A 100–200 MHz RF generator capable of over 50 W was designed and built to power these capillary devices. Time-averaged electron densities of 8×10^{14} cm^{-3} were observed via Stark broadening of hydrogen's Balmer lines when capillary plasmas were driven at 140 MHz with pressures ranging 30–300 Torr.

CHAPTER 2

THEORY

2.1 General Plasma Theory

Most matter in the universe is plasma. Plasma makes up interstellar winds and stars. On earth, plasma lights nearly every street and is involved in processing nearly every circuit. Plasma engineering has grown swiftly in the past sixty years since the advent of the integrated circuit and lasers, many of which use plasmas as their gain medium.

The following sections introduce basic plasma theory, emphasizing the interaction of plasmas and electromagnetic radiation that dominates plasma antenna operation.

Quasi-neutrality and the EEDF

Plasma is quasi-neutral: $n_e \approx n_i$, where n_e is the electron density and n_i is the ion density. These charged particles move freely in random directions, but, in bulk, plasmas are electrically neutral. Capillary plasma discharges like those presented in this thesis are low temperature, weakly ionized plasmas. *Weakly ionized* means that only a small fraction of the background gas is ionized ($n_e \approx n_i << n_g$, where n_g is the background gas density). Low-temperature plasmas are characterized by a non-equilibrium temperature distribution. The electron temperature is much higher than both the ions and the neutral gas species, $T_e >> T_i \approx T_g$ [5]. High-temperature plasmas which arrive at thermal equilibrium will not be discussed in this thesis.

T_e, T_i, and T_g are characteristic temperatures for a distribution of possible particle velocities. The probability of a particle having a given temperature is given by its energy distribution function. The most important energy distribution function in plasmas is the electron energy distribution function,

or EEDF, since electrons are the most mobile species with the highest energies in low-temperature plasmas. Their high energies and mobility allow electrons to participate in more processes and reactions than ions and neutral species. The EEDF is vital to calculating rate constants for ionization, momentum transfer, and excitation processes, many of which have threshold energies above 10 eV and require energetic particles to occur.

Electron, ion, and neutral gas densities, as well as each species temperature, serve to characterize a plasma discharge and dictate reaction rates, conductivities, and how plasmas interact with electromagnetic radiation, the topic of the next section.

2.2 Plasma and Electromagnetic Wave Interactions

Understanding the interaction between plasmas and electromagnetic waves is vital to engineering plasma antennas. A plasma discharge can behave like either a dielectric or a conductor with respect to an electromagnetic wave depending on the plasma frequency and the frequency of the electromagnetic wave.

The Plasma Frequency

In plasma discharges, the plasma frequency is the frequency of an undriven oscillation of a cloud of electrons about stationary ions. If a cloud of electrons is displaced, creating a local charge imbalance, electromagnetic forces between the electrons and the uncovered ions will produce an oscillation resembling a mass on a spring. The plasma frequency is the resonant frequency of this oscillation, given by the following expression [5]:

$$\omega_{pe} = \left(\frac{e^2 n_e}{\epsilon_o m_e} \right)^{1/2} \tag{2.1}$$

The electron density is n_e, ϵ_o is the permittivity of free space, m_e is the mass of an electron, and e is the charge of a single electron. The equation for the plasma frequency is intuitively satisfying. Plasmas with increased charged-species densities oscillate more rapidly, as the attractive force between the

electron and ion clouds increases with the charge density.

Plasma oscillations driven by a sinusoidally varying electric field can be used to calculate a plasma's response to incident electromagnetic radiation. If the ions are assumed to be stationary, the total current in 1D can be solved for with respect to the driving field, and a plasma dielectric constant can be extracted [5]:

$$\tilde{J}_{Tx} = j\omega\epsilon_o\left[1 - \frac{\omega_{pe}^2}{\omega(\omega - jv_m)}\right]\tilde{E}_x \tag{2.2}$$

$$\epsilon_p = \epsilon_o\left[1 - \frac{\omega_{pe}^2}{\omega(\omega - jv_m)}\right] \tag{2.3}$$

The plasma dielectric constant depends on the plasma frequency, ω_{pe}, the angular frequency of the incident field, ω, and the electron-neutral collisional frequency, v_m. It is complex-valued, indicating that if the collisional frequency is on the order of ω, the plasma will absorb incident radiation. If the electron-neutral collisional frequency is negligible and ω is less than ω_{pe}, the bulk plasma will behave like a metal with a negative dielectric constant, reflecting the incident radiation [6]. The radiation will penetrate to a certain skin depth, exponentially decaying in the bulk plasma. Surface waves at the plasma dielectric interface, however, can support surface waves from 3 MHz to over 1 GHz [6].

Physically, when the plasma frequency is greater than the frequency of the incident radiation, the electrons in the bulk plasma are able to respond to the oscillating field completely. These oscillating electrons both absorb and radiate additional electromagnetic fields. This response also occurs in metal, where electrons in the conduction band are free to accelerate in the incident field. However, when the reverse is true ($\omega_{pe} << \omega$), the electrons in the bulk plasma are not able to respond quickly enough and the incident radiation passes through; the plasma behaves like a dielectric.

In order for a plasma to behave like a metal, and therefore as an antenna, the incident electromagnetic frequency and the plasma frequency must be greater than the electron-neutral collisional frequency. In addition to this, the frequency of the incident radiation must be less than the plasma frequency. These two conditions are summed up in the expression $v_m << \omega << \omega_{pe}$ and shown in Fig. 2.1.

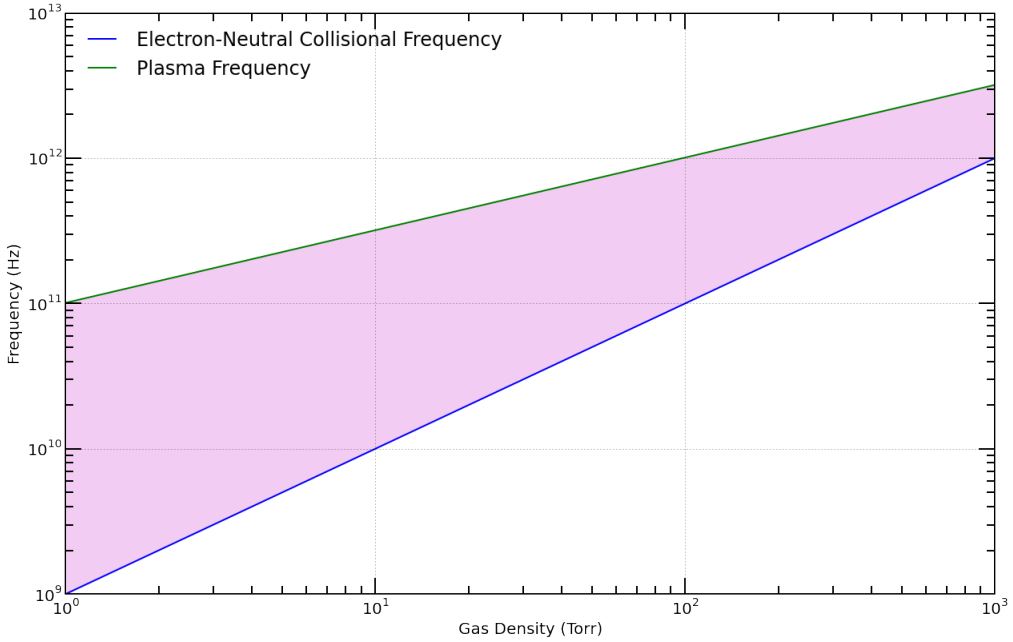

Figure 2.1: Comparison of the electron-neutral collisional frequency, v_m, and the plasma frequency, ω_{pe}. The magenta portion shows the frequencies of electromagnetic radiation over which the plasma behaves like a metal.

Plasma Conductivity

Like metals, plasma antennas use the distribution and flow of current on an antenna element to dictate the directivity and power of an antenna. In order to maintain adequate current, both metals and plasmas must have sufficiently high conductivities, which depend on n_e. The real part of the plasma conductivity is directly proportional to the electron density and inversely proportional to the electron-neutral collisional frequency, v_m, and the angular frequency of the incident radiation, given by the following expression:

$$\sigma_p = \frac{e^2 n_e v_m}{m_e(\omega^2 + v_m^2)} \tag{2.4}$$

Copper's conductivity is on the order of 50 MS/m. A plasma discharge with a gas density of 200 Torr, 10^{14} cm^{-3} electrons, at 1 GHz gives a conductivity of 14 S/m. Clearly plasmas, due to their lower number of electrons, have a lower conductivity. However, if sufficient electrons are present for a plasma to behave as antennas, other factors make up for this drawback.

Lower collision rates of electrons in the driving current with ions and neutral gas atoms reduce noise.

The Sheath Region

The sheath region that forms near the surface introduced into a plasma is important in all plasmas as all plasmas interface with other materials. The sheath region exists to balance the electron and ion flux at surfaces within a plasma. Due to their lower mass, electrons move more quickly than ions. While in the bulk plasma this disparity in velocity averages out, near surfaces the disparity causes a charge imbalance. The swift electrons reach the surface first and ions are slow to follow.

This charge imbalance creates an electric field directed toward the surface that accelerates ions towards the surface and slows electrons down until both charged species, at the surface, have the same flux. The acceleration of heavy ions in the sheath region is one of the main sources of power dissipation in a plasma, especially small-volume plasmas with high surface-to-volume ratios like the capillary microplasma discharges presented in this thesis.

2.3 Capacitively-Coupled Discharges

Plasmas require an energy source to sustain them. Common methods of generating and sustaining plasmas are DC excitation, capacitively or inductively coupled sources, and laser induced breakdown. The choice of driving mechanism sets a variety of parameters, including the electron density [5]. This work uses time-varying currents and voltages at frequencies between 20 kHz and 200 MHz to heat the plasma. The time-varying voltages can be coupled through a dielectric barrier or with electrodes directly in contact with the discharging gas species.

Plasma dynamics are complicated, with multiple atomic and molecular species interacting not only in the bulk plasma, but also in the sheath regions that form at surfaces or barriers within the plasma, and even with those surfaces themselves. In order to simplify the plasma dynamics, a simple model of a capacitively coupled discharge is introduced [5]. In this model, two parallel plates are separated by a distance, l. A time-varying voltage is

placed across the two plates. In the bulk plasma between the two plates, the electron and ion densities are roughly equal, following quasi-neutrality. At each of the two plates, two sheath regions exist, one instantaneous and the other time-averaged.

A few assumptions, which will be used later to estimate the power required to discharge capillary plasma devices at different frequencies, are as follows. First, the ions respond only to the time-averaged potentials between the plates. With respect to the electrons and the instantaneous time-varying potentials, the ions are assumed to be stationary. Second, the electrons respond to the instantaneous time-varying potentials. This is a good approximation if the following is true [5]:

$$\omega_p^2 >> \omega^2\sqrt{1+\frac{v_m^2}{\omega^2}} \tag{2.5}$$

where ω_p is the plasma frequency, ω is the angular driving frequency, and v_m is the electron-neutral collisional frequency (which can be obtained from the rough empirical formula, $v_m \approx P \times 10^9$ Hz, where P is the pressure in Torr). This condition holds for electron densities above 10^{12} cm^{-3}. However, if one were to lower the frequency to 20 kHz, the lower bound on driving frequency for this work, this condition holds true for electron densities as low as 10^8 cm^{-3}.

2.4 Estimating the Electron Temperature, Electron Density, and Power Deposition in a Capillary Plasma Discharge

The most important plasma parameter in this thesis is the electron density, which dictates how plasmas respond to incident electromagnetic radiation, which is the fundamental interaction for antenna operation. A simplified model of a capillary discharge with cylindrical geometry will be presented and used to calculate the electron temperature and the power required to sustain a discharge of a given electron density. These calculations were used to guide the construction of an RF source used in subsequent experiments.

The simplified model assumes a cylindrically symmetric discharge volume

with a diameter, d, and length, l, with electrodes as end caps. Neon is assumed to be the discharge medium. A DC electric field is placed across the tube, and the DC voltage is assumed to be roughly equal to the rms value of an RF source.

Electron Temperature

The electron temperature in a plasma discharge is set by the geometry of the discharge. In order to maintain a plasma in steady state, this model proposes a simple electron continuity equation that balances electron losses to the walls due to diffusion with direct electron impact ionization, or:

$$\frac{\partial n_e}{\partial t} = n_e K_{ion} n_g - \frac{D_a}{\lambda^2} = 0 \tag{2.6}$$

$$\lambda = \frac{d}{2 \cdot 2.405} \tag{2.7}$$

$$D_a = D_{ion}(1 + \frac{T_e}{T_g}) \tag{2.8}$$

where D_a is the ambipolar diffusion coefficient, λ is geometrical scaling factor, n_g is the neutral gas density, n_e is the electron density, and K_{ion} is the direct electron-neutral ionization rate coefficient (cm^3/s) [7].

The first term on the right-hand side of Eqn. 2.6 gives the number of electrons generated by direct electron impact ionization in a given time. It is directly proportional to the density of available electrons accelerated in the DC field, the number of neutral atoms present, and the direct electron impact ionization rate coefficient. Rate coefficients are the average of the product of interaction cross-sections and the velocity of the species in question, or $k = < \sigma v >$. Cross-sections for various processes, from momentum-transfer collisions to non-ionizing excitations and ionization collisions, can be obtained from the literature. The velocity of electrons depends on their temperature, which is given by the electron energy distribution function (EEDF), $f(E)$. The explicit calculation for the rate coefficient is:

$$k = \int_0^\infty f(E) \left(\frac{2E}{m_e} \right)^{1/2} \sigma(E) \mathrm{d}E \tag{2.9}$$

For calculation simplicity, the EEDF is assumed to be a Maxwell-Boltzmann distribution. The magnitude of neon's direct impact ionization cross-section was taken from Rapp and Englander-Golden's compilation of electron impact ionization in noble gases [8] and approximated with a step function in energy.

The generation of electrons due to direct impact ionization is balanced by diffusion losses to the walls of the cylindrical tube. D_a is the ambipolar diffusion coefficient that gives the overall diffusion of electrons and ions towards the wall. Like in the sheath region, electrons diffuse more quickly than ions to the walls of the chamber whose normal vector is perpendicular to the direction of the imposed field. As the electrons move to the walls, an electric field is generated by the charge separation induced by the differences in flux. This electric field retards electrons and accelerates ions, producing a scaled diffusion coefficient. Eqn. 2.8 describes this relationship: the hotter the electrons, the stronger the induced electric field, and the stronger acceleration of ions toward the wall.

In Fig. 2.2, loss of electrons due to ambipolar diffusion and gains from ionization are plotted with respect to their mutual variable, the electron temperature. The two processes balance where they intersect, producing steady-state conditions at electron temperatures ranging from 0.2 to 2 eV for tubes with diameters from 0.5 mm to 1 cm. As can be seen, the diameter of the tube sets the steady-state electron temperature in cylindrical discharge.

This estimate of the electron temperature is only approximate. The EEDF is not necessarily a Maxwell-Boltzmann distribution, and the direction-ionization cross-section is not a step function. Other sources and sinks of electrons and ions are likely present as well. However, these assumptions provide an estimate of the electron temperature that is of the same order as those reported in the literature [9].

Power Deposition

For a given electron temperature, T_e, electron density, and volume of discharge, one can estimate the power needed to sustain a plasma with the following equations:

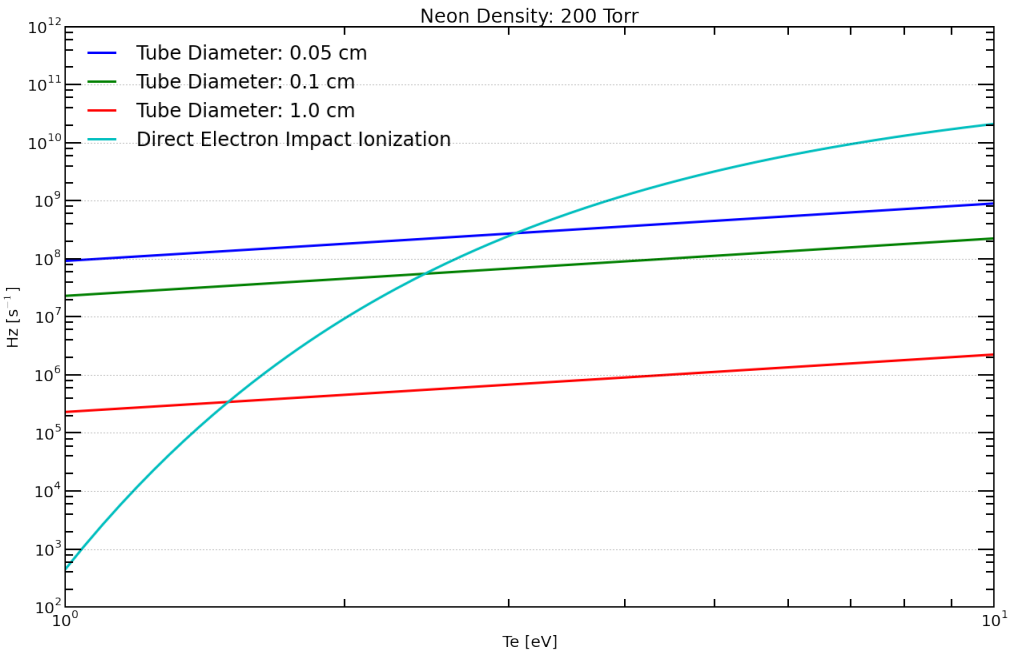

Figure 2.2: For 200 Torr of neon and a cylindrical tube with diameters of 500 μm, 1 mm, and 1 cm. The electron temperatures at steady state are where the ambipolar diffusion and ionization intersect, and are roughly between 0.2 and 2 eV.

$$P(T_e) = \int_0^\infty f(E)\left(\frac{2E}{m_e}\right)^{1/2}\sigma(E)\Delta E\mathrm{d}E \tag{2.10}$$

$$P_{tot} = P(T_e)n_eNV \tag{2.11}$$

where ΔE is the energy loss by an electron per collision, and V is the volume of the discharge. In the case of direct impact ionization, the energy loss per collision is assumed to be the ionization energy of the gas species, in this case neon. The total power dissipated in a few selected volumes with respect to electron temperature is presented in Fig. 2.3.

The 100–200 MHz RF source fabricated to discharge capillary plasma devices designed with Fig. 2.3 in mind. A maximum power of 100 W was decided upon, taking into consideration the lack of a matching network and the considerable losses due to the impedance mismatch between the guided incident power and the plasma itself.

Now that the characteristics of the plasma itself have been discussed, the

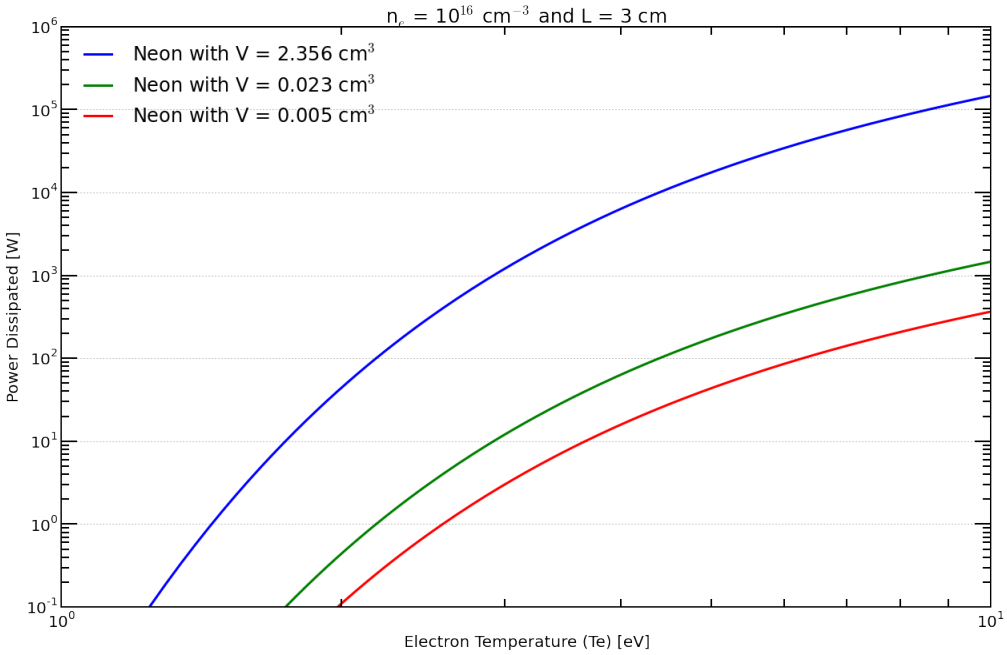

Figure 2.3: Calculated power dissipation in a cylindrical tube with a length of 3 cm and diameters of 500 μm, 1 mm, and 1 cm. Electron density is assumed to be 10^{16} cm^{-3}, the upper limit seen in Hoon's simulations [4].

interaction of the discharge with electromagnetic radiation will be addressed.

2.5 Spectroscopic Measurement of Electron Density

Both the plasma frequency and the conductivity of a plasma discharge depend on the electron density. Antenna operation requires as high a conductivity as possible. The basic engineering challenges in this thesis are to properly characterize the electron density in a discharge, increase the fractional ionization of the plasma discharge to increase the conductivity, and increase the duty cycle of the plasma discharge during operation. In this thesis the plasma discharge occurs in a small volume, with an inner diameter of less than 1 mm, so conventional methods for measuring the electron density, such as Langmuir probes, are unfeasible.

The measurement of Stark broadening of hydrogen's Balmer series is a spectroscopic technique to estimate a plasma's electron density. However, since the glass and quartz tubes used to contain the discharges are trans-

parent in the visible, these devices are well suited to characterization via spectroscopic techniques.

This phenomenon is based on the Stark effect, which is the impact of a local electric field on the energy levels of hydrogen-like atoms. For example, the Balmer series in hydrogen, which are the transitions from energy levels with the principle quantum numbers above 2 (n $>$ 2) that terminate on the second excited state ($n = 2$), are typically degenerate. Two electrons share the same energy, differing only in their spin. In the presence of a local electric field, the hydrogen atom is polarized, and the resulting dipole moment interacts with the two spins differently, causing the energy levels for the two states to shift up and down. In hydrogen, the Stark broadening dominates over Doppler broadening due to its strong linear effect [10]. In a plasma, the higher density of electrons produces stronger local electron fields (within a Debye length), and therefore broadening in the Balmer lines can be readily observed.

Due to the utility of Stark broadening measurements of hydrogen in plasma diagnostics, [10] and [11] compiled experimental and theoretical tables that correlate the FWHM of a Balmer line with electron density. Since Stark broadening is Lorentzian, experimental data can be fit with a Lorentzian lineshape, and the FWHM can be extracted to give electron density estimates.

CHAPTER 3

EXPERIMENT

The experimental results for two capillary plasma discharges will now be discussed. Both capillary devices share common features. The capillary tubes are between 3 and 5 cm long with inner diameters between .5 mm and 1.1 mm. Electrodes for both devices were placed outside, capacitively coupling an AC voltage through a dielectric barrier.

Two main characteristics distinguish the two devices. The driving frequencies of the devices differ by two orders of magnitude. The first device, constructed with a borosilicate glass tube, uses frequencies of 10–40 kHz. This low-frequency operation leads to discharges characterized by short-lived current and electron density spikes and consumes milliwatts in power. In order to increase the electron density in these capillary discharges, higher frequency driving voltages were proposed, operating at over 1 MHz in accordance with [4]. In order to accommodate the higher frequencies, the dielectric material of the capillary tube was changed from glass to alumina and quartz.

3.1 Experimental Setup

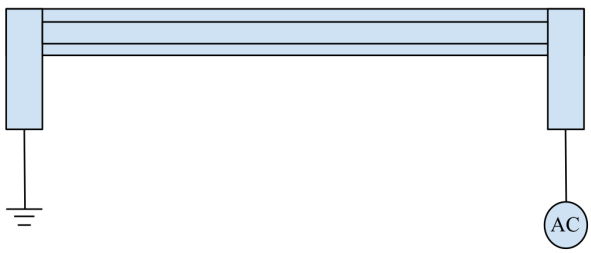

Figure 3.1: Basic diagram of a capillary plasma discharge.

The basic discharge schematic for both the borosilicate and alumina tubes

is presented in Fig. 3.1. The electrodes on the capillary tubes are made from either copper tape or silver epoxy. All experiments were conducted on optical tables with metal surfaces; these surfaces served as ground for the ground electrode and the AC signal.

The capillary tubes were connected via Ultra-Torr fittings to a vacuum system capable of base pressures of 10^{-7} Torr. An MKS Instruments 626 Absolute Capacitance Manometer measured the pressure from 1 to 1000 Torr while an ion gauge measured all lower pressures. A gate valve separated a high-vacuum volume while capillary tubes were filled and discharged. Manual ball values were used for gas inlet.

Different noble gases were used in the capillary discharges, the predominant species being neon and argon. During Stark broadening measurements, a 1% mix of hydrogen was added to the discharge. Capillary discharges occurred at pressures ranging from 500 mTorr to 700 Torr, depending on the voltage applied and the cleanliness of the tube.

3.2 Borosilicate Tubes Driven by 20 kHz Sinusoidal Voltage

In order to generate 10–40 kHz signals, an audio amplifier boosts the output of a function generator, which in turn is amplified by a step-up transformer. The amplification chain is capable of producing 5 kV amplitude waveforms. Ground and high-voltage cables are attached to the copper tape or silver epoxy leads in Fig. 3.1. To measure the current, an inductive current probe is placed on the ground lead. A high-voltage probe is used to measure the voltage waveform across the capillary discharge device. Fig. 3.2 shows a characteristic set of voltage and current waveforms present during device operation. Current and electron density are roughly proportional, given the following relationship [7]:

$$j = \sigma E = \frac{e^2 n_e}{m_e \upsilon_m} E \tag{3.1}$$

The FWHM of the peak current pulse, superimposed on the sinusoidal capacitive current, is less than a microsecond, indicating a $\sim$1% duty-cycle.

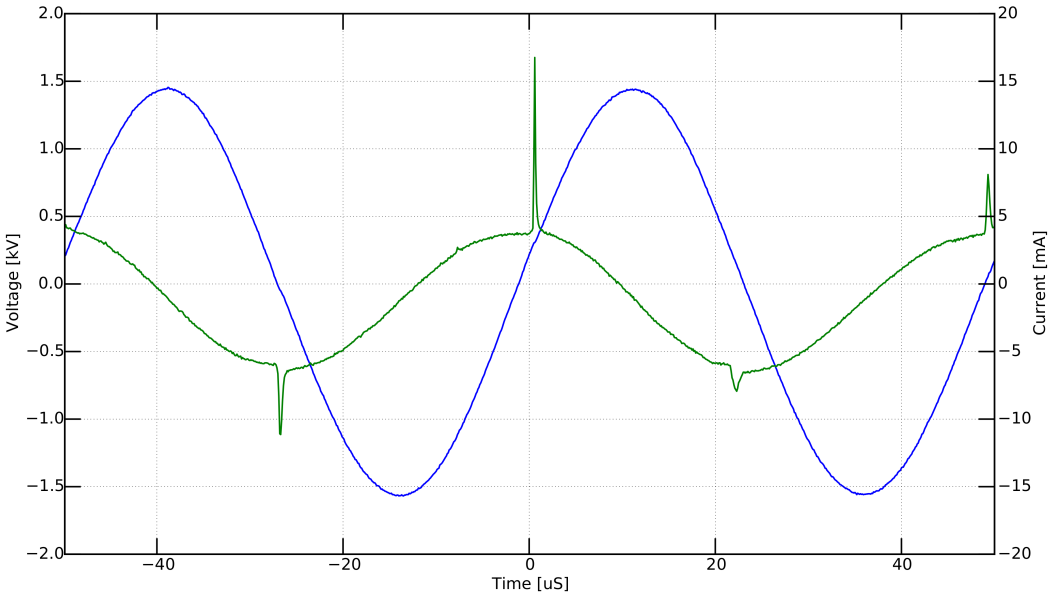

Figure 3.2: Driving voltage and current of a glass capillary plasma with 200 Torr neon.

In order to improve the performance of the capillary discharges, broadband measurement of the spectrum in the visible region (300–1000 nm) was used to check the discharge for impurities due to adsorption of impurities in the tube walls while exposed to air, or to leaks in the vacuum setup itself. Most of the impurities observed, as in Fig. 3.3, were due to the presence of water vapor and would diminish as stock gas was cycled from 10 mTorr back up to the operating pressures of 50–200 Torr.

The measurement of the H-α line with an ICCD and spectrometer capable of measuring down to 0.5 Å was performed in order to estimate the electron density. The capillary discharge was placed immediately at the entrance slit of the spectrometer. The ICCD was gated and triggered to measure a particular Balmer line when peak intensity occurred, which was found manually. Many accumulations were integrated in order to get an adequate signal of the Balmer lines in question. As mentioned in Section 2.4, the FWHM of the H-α and H-β Balmer lines in hydrogen have been tabulated in [10] and [11]. In Fig. 3.4, H-α was measured and fit with a Lorentzian lineshape which has a FWHM of 1.53 Å. This corresponds to an electron density of 10^{15} cm^{-3} and a conductivity of approximately 140 S/m, which is adequate for a plasma antenna. However, this conductivity and electron

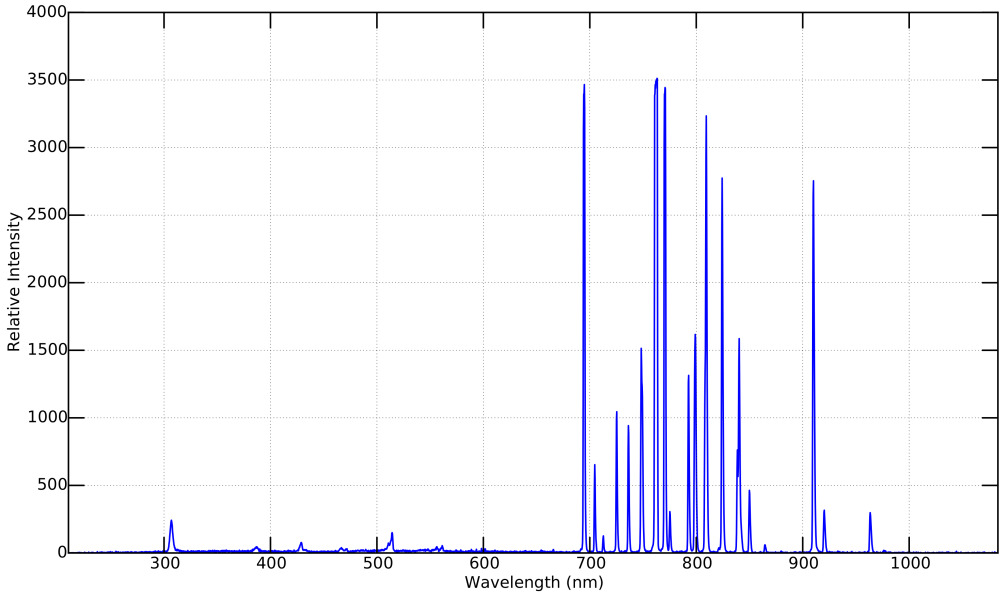

Figure 3.3: Broadband spectra of neon at 200 Torr, 5 kVp-p discharge in a glass tube with 1 mm ID. Lines at 300 nm show impurities just after initial discharge. Cycling the discharge gas repeatedly purged the impurities from the device.

density are not time-averaged values. The gate used to measure the Stark broadening was 100 ns. Therefore, the calculated time-averaged electron density is 10^{12} cm^{-3} and the conductivity is $\sim$.14 S/m.

Once these measurements were taken, the borosilicate capillary devices were sealed with a butane torch. The pressure during the seal-off procedure was observed in order to ensure a clean glass seal.

An additional check of the electron density, performed with Dr. Abbas Semnani at Purdue University, was to integrate capillary discharges into antenna structures that had been theoretically characterized for given electron densities. A network analyzer was used to measure the S11 parameter of the resonant structures and was compared with the theoretical calculations. A horizontal dipole antenna operating in neon at 200 Torr, with a 1 mm ID, was installed over a 5 cm ground copper ground plane. It was expected to have a peak S11 of -37 dB at 2.45 GHz if a time-average of 10^{16} cm^{-3} electrons were present [12]. When no discharge was present the structure had a lower S11 value peaked at about 5 GHz. During experimental testing, the capillary discharges were energized, but no shift in the S11 parameter was observed, confirming that the time-averaged value of the electron density was

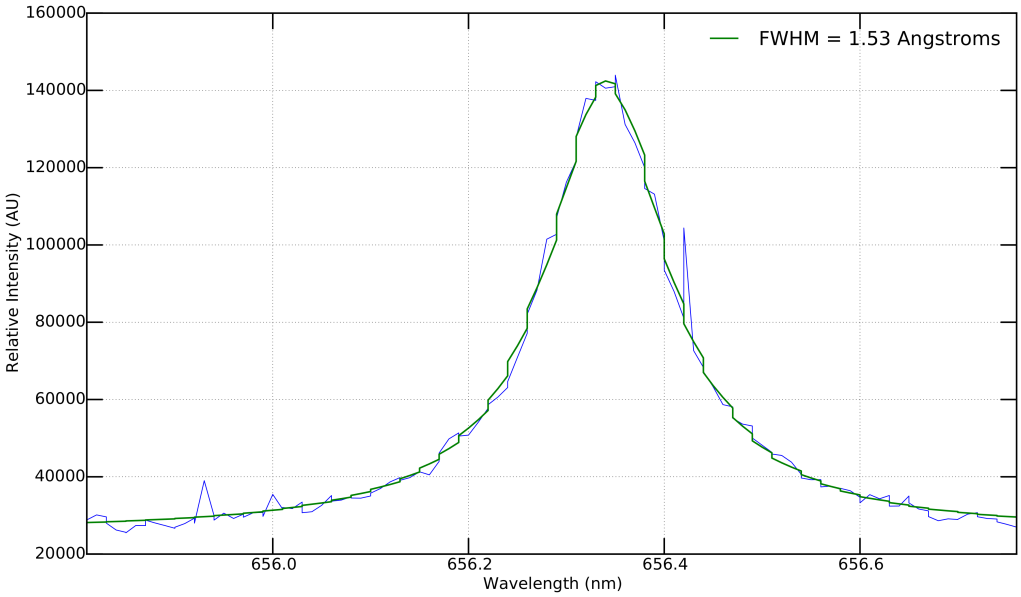

Figure 3.4: H-α broadening in neon at 200 Torr, 5 kVp-p discharge in a glass tube with 1 mm ID. A Lorentzian fit is superimposed over the data. The extracted 0.153 nm FWHM from the Lorentzian fit corresponds to an electron density of 10^{15} cm^{-3}.

lower than needed.

3.3 Quartz Tubes Driven by 140 MHz RF Generator

In order to increase the time-averaged electron density, higher frequency operation, suggested by [4], in the range of 100–200 MHz was implemented. In order to accommodate higher power operation, ceramic and quartz tubes were used, as both have significantly higher melting points than borosilicate. However, the majority of devices used quartz, since quartz is optically accessible.

A 100–200 MHz RF generator was constructed with the following chain: voltage controlled oscillator (VCO), voltage variable attenuator (VVA), high-power RF amp, circulator, and dual directional coupler (DDA). The schematic of this generator is shown in Fig. 3.5. The DDA couples out 40 dB from the forward and backwards propagating RF power into detectors to measure the incident and reflected power. The circulator redirects any reflected power into a 100W RF load to protect the power amplifier, VVA, and VCO. A mi-

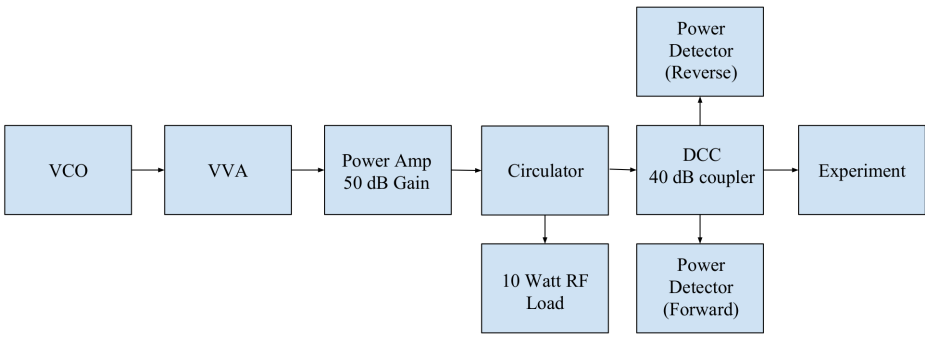

Figure 3.5: Schematic for the 100–200 MHz, 100 W RF generator.

crocontroller's PWM 0–5 V analog output was filtered and amplified to 0–12 V and used to control the VCO. A function generator was used to control the VVA, with a 0–5 V control voltage controlling attenuation from 40 to 10 dB.

The quartz tube, with an inner diameter of 900 μm, used the same electrode configuration as in Fig. 3.1. The quartz tube was attached to a 1/4 inch glass tube via an aluminum reducer, and the tube opening and joints between the quartz tube, the reducer, and the 1/4 inch glass tube were cemented with Torr Seal. Short high-voltage cables connect the center pin of the coaxial cable to the high-voltage electrode while the aluminum reducer connects to ground.

In order to initiate discharge, a 140 MHz, >10 W CW RF signal incident on a quartz tube backfilled with 30-60 Torr of neon was boosted by a Tesla coil to provide the initial electron avalanche. Once ignited, the capillary plasma would remain energized in neon. Argon discharges had power oscillations that sometimes led to self-extinguishing.

Both neon and argon capillary plasmas showed increased intensity with increased peak-to-peak voltages. The recorded broadband spectra (a reference image is shown in Fig. 3.6) showed very few impurities in the 300–600 nm spectral region. However, at peak-to-peak voltages over 110 V spectral features indicating the presence of molecular species appear. In Fig. 3.7, the voltage and current waveforms representative of discharges driven by 140 MHz are shown. In contrast with Fig. 3.2, the MHz current waveform shows no current spikes representative of a filamentary discharge, indicating that these capillary discharges operate in the glow mode.

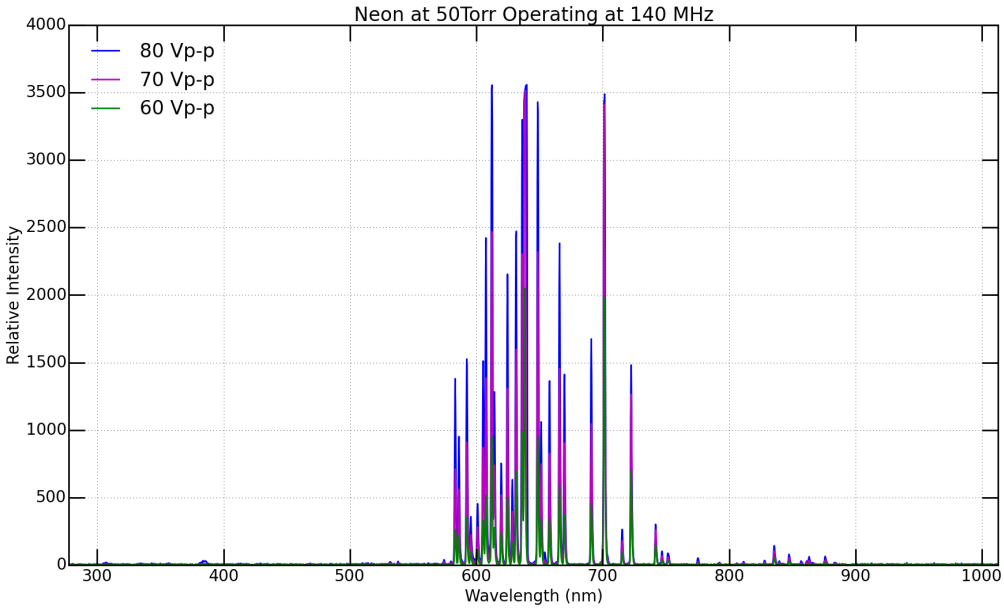

Figure 3.6: Broadband spectra of neon at 50 Torr, 140 MHz RF signal with varying input powers, as shown by different peak-to-peak voltages. Impurities are not spectrally present.

Stark broadening measurements were also conducted for argon and neon discharges ranging from 30 to 300 Torr. The same ICCD setup was used to measure the electron density. However, a 10 μm gate width was used, which covered thousands of cycles of RF power, and therefore the resulting measurements were time-averaged. This direct measurement of the time-averaged electron density was possible due to the much greater intensity of emission in the RF driven capillaries. As shown in Fig. 3.8, the time-averaged electron density was measured to be 8×10^{14} cm^{-3}, confirming that these devices are capable of operating as monopole antenna elements.

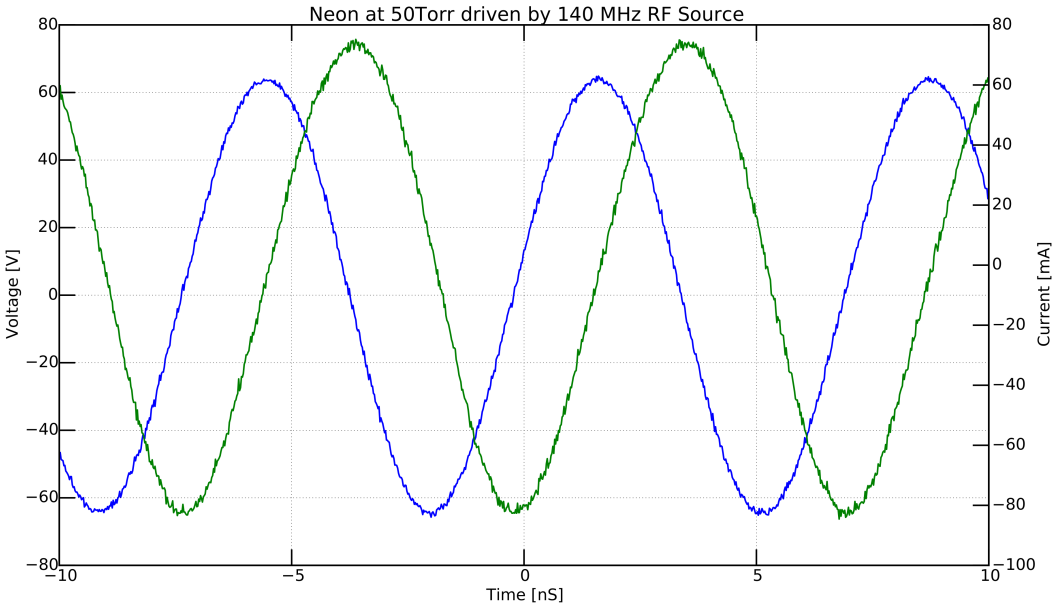

Figure 3.7: Voltage and current waveforms for a capillary discharge in neon at 50 Torr, driven by a 140 MHz RF signal. The voltage is in blue, and the current is in green.

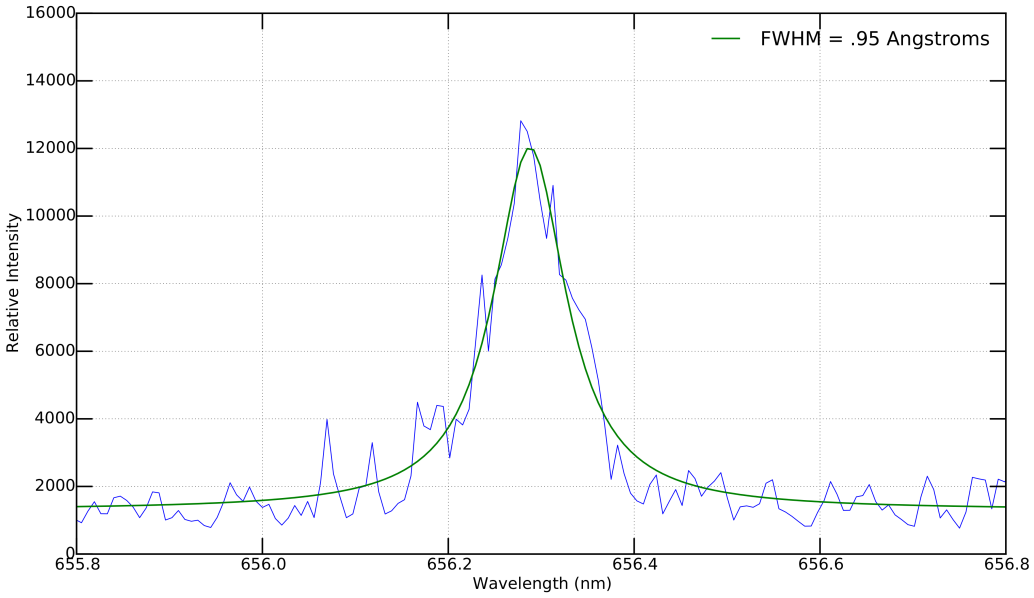

Figure 3.8: Stark broadening measurement of the H-α Balmer line in 300 Torr of argon. The FWHM of 0.95 nm corresponds to an electron density of 8×10^{14} cm^{-3}.

CHAPTER 4

CONCLUSIONS

Plasma antennas using microplasma monopole elements require electron densities greater than 10^{14} cm^{-3} and conductivities of 100 S/m. This thesis demonstrates that capillary microplasma antenna elements will work if driven at sufficiently high frequencies, recording time-averaged electron densities of 8×10^{14} cm^{-3}. Future work to improve these devices includes improving the plasma breakdown characteristics, shrinking the footprint of the driving circuit, characterizing the pressure and voltage characteristics, measuring the IV curves, and minimizing the power requirements to drive these elements.

REFERENCES

[1] W. Jiayin, S. Jiaming, W. Jiachun, and X. Bo, "Study of the radiation pattern of the unipole plasma antenna," in *2006 7th International Symposium on Antennas, Propagation & EM Theory*. IEEE, 2006, pp. 1–4.

[2] W. L. Stutzman and G. A. Thiele, *Antenna Theory and Design*. John Wiley & Sons, 2012.

[3] T. Anderson, *Plasma Antennas*. Artech House, 2011.

[4] S. H. Sung, "Coupled phenomena in arrays of microplasma devices and microchannel plasma devices as antennas," Ph.D. dissertation, University of Illinois at Urbana-Champaign, 2011.

[5] M. A. Lieberman and A. J. Lichtenberg, *Principles of Plasma Discharges and Materials Processing*. John Wiley & Sons, 2005.

[6] G. Borg, J. Harris, N. Martin, D. Thorncraft, R. Milliken, D. Miljak, B. Kwan, T. Ng, and J. Kircher, "Plasmas as antennas: Theory, experiment and applications," *Physics of Plasmas (1994-present)*, vol. 7, no. 5, pp. 2198–2202, 2000.

[7] T. Houlahan, Course Notes, ECE 523: Gaseous Electronics and Plasmas, University of Illinois at Urbana Champaign, 2014.

[8] D. Rapp and P. Englander-Golden, "Total cross sections for ionization and attachment in gases by electron impact. I. positive ionization," *Journal of Chemical Physics*, vol. 43, no. 5, pp. 1464–1479, 1965.

[9] J. P. Rayner, A. P. Whichello, and A. D. Cheetham, "Physical characteristics of plasma antennas," *IEEE Transactions on Plasma Science*, vol. 32, no. 1, pp. 269–281, 2004.

[10] H. R. Griem, A. C. Kolb, and K. Shen, "Stark broadening of hydrogen lines in a plasma," *Physical Review*, vol. 116, no. 1, p. 4, 1959.

[11] M. A. Gigosos and V. Cardeñoso, "New plasma diagnosis tables of hydrogen stark broadening including ion dynamics," *Journal of Physics B: Atomic, Molecular and Optical Physics*, vol. 29, no. 20, p. 4795, 1996.

[12] A. Semnani, private communication, 2015.